Chapter 8

Nuclear Effects in Non-Singlet Structure Functions and Sum Rules

In this chapter we present an analysis of the non-singlet structure functions and related sum rules taking into account the nuclear effects. In this regard, special attention is given to the nuclear shadowing effect as we are mostly concerning with the small-x region. The corrections due to nuclear shadowing effect, predicted in several earlier analysis are incorporated to our results of structure function and sum rules for free nucleon and calculate the nuclear structure functions as well as sum rules for nuclei. The calculations are analysed phenomenologically in comparison with available experimental data and achieved at a very good phenomenological success in this regard.

8.1 Introduction

Higher order pQCD corrections have a significant contribution towards the precise predictions of the structure functions as well as the sum rules. In the Chapters 4, 5, 6 and 7 we have discussed in detailed about the evolution of non-singlet structure functions and associated sum rules in accord with pQCD, along with their QCD corrections up to NNLO. In addition to pQCD corrections there are several non-perturbative effects such as higher twist effects, nuclear corrections, target mass corrections etc., to be included into the joint QCD analysis of structure functions and sum rules. In this chapter we present an analysis of the non-singlet structure functions and related sum rules taking into account the nuclear effects. Particular emphasise is given to the

shadowing effect as we are mostly dealing with the small-x region.

We have already given a brief introduction about the nuclear effects in section 1.7. The fact that the structure functions of bound and free nucleons are not equal was discovered in a deep inelastic muon experiment carried out by the European Muon Collaboration at CERN in 1982[52]. Since then the nuclear effect has been actively investigated with ever more sophisticated and ingenious deep inelastic scattering experiment with charged lepton and neutrinos.

Available experimental information on nuclear structure functions are mainly from charged-lepton scattering DIS experiments performed at CERN [180–186], SLAC [187, 188], DESY [189], FNAL[190, 191] and recently at JLab [192, 193]. In addition, data from the DrellYan reaction of protons off nuclear targets are also available [194]. The experiments usually measures the ratio R_2 of the structure function F_2 of a complex nucleus to deuterium. The studies on the behaviour of the ratio R_2 as a function of x for a given fixed Q^2 reflects four distinct region of characteristic nuclear effects: shadowing region($x < 0.1$), anti-shadowing region($0.1 < x < 0.3$), EMC region ($0.3 < x < 0.8$) and fermi motion region($x > 0.8$). In addition there are several theoretical treatments that predicts a Q^2 dependent nuclear effect only in the shadowing region, while for $0.1 < x < 0.8$ R_2 is almost Q^2 independent. However, the data available on the Q^2 dependence of nuclear effects are still scarce. In this thesis we have not take into account the Q^2 dependent nuclear corrections and considered only the x-dependency of nuclear effects for structure functions.

A quantitative understanding of the nuclear effects in deep inelastic nuclear scattering is important for a number of reasons. A proper interpretation of experimental data can provide valuable insights into the origin of nuclear force and helps us in understanding the possible modification of the properties of hadrons in a nuclear medium. Further, nuclear data provides the opportunity to have reliable information on the hadrons, otherwise not accessible directly. As for example, the extraction of the neutron structure function usually requires the deuterium and proton data, which in turn requires a proper understanding of nuclear effects[195]. Similarly, the use of charged-lepton and neutrino nuclear DIS data in global analysis of QCD observables aiming towards better determination of the proton and neutron pdfs and the higher twist terms [196–198] are the other examples in this regard.

The understanding of nuclear effects is particularly relevant for neutrino physics. For precision measurements in neutrino physics the use of heavy nuclear targets is

required in order to collect a significant number of interactions. The presence of an axial-vector component in the weak current and the quark flavour selection distinguishes neutrinos from charged leptons and imply a more complex description of nuclear effects in neutrino scattering. The role of nuclear corrections to neutrino structure functions has been recently emphasized[199] after the NuTeV collaboration reported a deviation from the Standard Model prediction for the value of the weak mixing angle ($sin^2\Theta_W$) measured in neutrino DIS [200]. It must be mention that nuclear effects are important not only in the determination of electroweak parameters, but also for the understanding of neutrino masses and mixing. The recent high-intensity NuMI[201] and JPARC [202] neutrino facilities offer the possibility to perform a detailed study of nuclear effects in neutrino interactions on a relatively short time scale. The construction of a future neutrino factories[203] are expecting to reach the ultimate precision of the neutrino probe.

8.2 Shadowing Effect in Nuclear Deep Inelastic Scattering

As this thesis is concerned with the small-x behaviour of the non-singlet structure functions and sum rules, we would like to concentrate only on the shadowing effect. Shadowing effect is the most pronounced nuclear effect in lepton nuclear DIS. Several theoretical models to this shadowing have been proposed. In literature there are essentially two main classes of approaches in order to have information about shadowing effect: one concerns with the origin of the shadowing effect and the other one addresses the evolution of shadowing effect by means of parameterizations.

Some models associated with the origin of shadowing effect provides a qualitative understanding using the fact that that in the rest frame of the nucleus the incoming photon splits into a $q\bar{q}$ pair long before reaching the nucleus, and this $q\bar{q}$ pair interacts with it with typical hadronic cross sections, which results in absorption [204–210]; in this way nuclear shadowing is a consequence of multiple scattering which in turn is related to diffraction [207, 211, 212]. On the other hand, in a frame in which the nucleus is moving fast, gluon recombination due to the overlap of the gluon clouds from different nucleons reduces gluon density in nucleus with mass number A by A times that in a free nucleon[213, 214]. These studies have received a great theoretical impulse with the development of semiclassical ideas in QCD and the appearance of

non-linear equations for evolution in x in this framework(see [215–217] and references therein.).

Other models do not address the origin of the nuclear shadowing but contains a parametrization at Q_0^2, which is obtained from a fit to experimental data. Distribution of partons inside nucleus are parameterized at some scale Q_0^2 and then evolved using the DGLAP[24] evolution equations. Nuclear effects are usually studied through a global χ^2 analysis method by using all the available charged-lepton DIS data, and then by adding Drell-Yan data to the data set[218]. In order to determine nuclear effects, various global analysis have been reported[219–224]. The analysis performed by Eskola et al.[225] and Hirai et al.[218, 224] are based on the leading-order(LO) Dokshitzer-Gribov-Lipatov-Altarelli-Parisi(DGLAP) evolution, while the next-to-leading-order (NLO) evolution was performed by de Florian and Sassot[219]. In 1999, Eskola, Kolhinen, Ruuskanen and Salgado(EKRS)proposed a set of nuclear parton distributions by using the F_2^A/F_2^D data in deep inelastic lA collisions and the nuclear Drell-Yan dilepton cross sections measured in pA collisions and their results were observed to agree very well with the relevant EMC data and the E772 data at Fermilab[226] within the kinematical ranges $10^6 \leq x \leq 1$ and $2.25GeV^2 \leq Q^2 \leq 10^4 GeV^2$. A reasonable explanation of the measured data of F_2 was provided by Hirai, Komano and Miyama(HKM)[224] based on two (quadratic and cubic) types of nuclear parton distributions whose parameters were determined by a χ^2 global fit to the available experimental data, except those from the proton-nucleus Drell-Yan process. The covered kinematical ranges were $10^9 \leq x \leq 1$ and $1GeV^2 \leq Q^2 \leq 105GeV^2$ for deuteron and heavy nuclear targets. Further, in 2004, Hirai, Komano and Nagai(HKN)[218] re-analyzed the measured ratios of nuclear structure functions $F_2^A/F_2^{A'}$ and the ratios of Drell-Yan cross sections between different nuclei for obtaining another parton distribution function in nuclei.

In Ref. [219–222] the nuclear parton distribution have been determined, whereas Ref. [223] concentrated on the determination of nuclear structure functions using conventional nuclear models. The results from different models usually depend on additional semi-phenomenological assumptions and often contradict each other. Some recent parametrization are provided bellow as examples

- FS04[219]($Q_0^2 = 0.4GeV^2$): $f_i^{N/A}(x) = \int \frac{dy}{y} W_i(y, A, Z) f_i^N(x/y)$

$$W_i(y,A,Z) = \begin{cases} A[a_v\delta(1-\varepsilon_v-y)+(1-a_v)\delta(1-\varepsilon'_v-y)] \\ +n_v(y/A)^{\alpha_v}(1-y/A)^{\beta_v}+n_s(y/A)^{\alpha_s}(1-y/A)^{\beta_s} \qquad (i=V) \\ A\delta(1-y)+\frac{a_i}{N_i}(\frac{y}{A})^{\alpha}_i(1-\frac{y}{A})^{\beta_i} \qquad (i=s,g) \end{cases}$$

- HKN07[220]($Q_0^2 = 1GeV^2$): $f_i^A(x) = W_i(y,A,Z)\frac{1}{A}[Zf_a^p(x)+(A-Z)f_a^n(x)]$
  $W_i(y,A,Z) = 1+(1-\frac{1}{A^\alpha})\frac{a_i+b_ix+c_ix^2+d_ix^3}{(1-x)^\beta}$

- SYKMOO08[221]($Q_0^2 = 1.69GeV^2$): $f_i^A(x) = W_i(y,A,Z)\frac{1}{A}[Zf_a^{p/A}(x)+(A-Z)f_a^{n/A}(x)]$
  $xf_i^{N/A}(x) = \begin{cases} A_0x^{A_1}(1-x)^{A_2}e^{A_3x}(1+e^{A_4}x)^{A_5} \qquad (i=u_v,d_v,g,\bar{u}+\bar{d},\bar{s}) \\ A_0x^{A_1}(1-x)^{A_2}+(1+A_3x)(1-x)^{A_4} \qquad (i=\bar{d}/\bar{u}) \end{cases}$

- EPS09[222] ($Q_0^2 = 1.69GeV^2$): $f_i^A(x) = R_i^A(x)\frac{1}{A}[Zf_a^p(x)+(A-Z)*f_a^n(x)]$,
  $R_i^A(x) = \begin{cases} a_0+(a_1+a_2x)[e^{-x}-e^{-x_a}] \qquad (x \le x_a : shadowing) \\ b_0+b_1x+b_2x^2+b_3x^3 \qquad (x_a \le x \le x_e : antishadowing) \\ c_0+(c_1-c_2x)(1-x)^{-\beta} \qquad (x_e \le x \le 1 : EMC\ and\ Fermi\ Motion) \end{cases}$

Here f_i^A is the nuclear parton distribution function for the parton type i and f_i^p and f_i^n are the corresponding proton and neutron contribution. The parameters in these equations are determined by global χ^2 analyses of world experimental data on nuclear structure functions. Experimental data are generally obtained in different Q^2 points from Q_0^2. The standard DGLAP evolution equations are used for evolving the distributions to the experimental points. There are three conditions to be satisfied for the NPDFs, so that three parameters should be fixed by the following relations [218, 224]:

- Baryon number: $A\int dx[\frac{1}{3}u_v^A(x)+\frac{1}{3}d_v^A(x)] = A$
- Charge: $A\int dx[\frac{2}{3}u_v^A(x)-\frac{1}{3}d_v^A(x)] = Z$
- Momentum:$A\sum_{i=q,\bar{q},g}\int dx x f_i^A(x) = A$

Like the charged-lepton DIS, the deep inelastic neutrino scattering is also a significant process for investigating the structures of hadrons and nuclei. In neutrino-DIS process, the structure functions $F_2(x,Q^2)$ and the parity-violating structure function $xF_3(x,Q^2)$ can simultaneously be measured. Big European Bubble Chamber Collaboration (BEBC) published the antineutrino-neon/deuterium DIS data in 1984, within the kinematic region of $0 < x < 0.7$ and $0.25 < Q^2 < 26GeV^2$[229]. BEBC results for differential cross section ratio in the high Q^2 and $0.3 < x < 0.6$ region[229] is

compatible with the muon and electron scattering data from EMC and SLAC. In the same year, CERN-Dortmund-Heidelberg-Saclay Collaboration (CDHS) measured events originating in a tank of liquid hydrogen and in the iron of detector in the 400 GeV neutrino wide-band beam of the CERN Super Proton Synchrotron(SPS)[230]. In their measurements on total cross sections, differential cross sections and structure functions for hydrogen and iron, no significant difference between the structure functions for proton and iron was observed. E545 Collaboration at Fermilab [231], once more measured the cross sections in the deep inelastic neutrino scattering on neon or deuterium. However they were not able to give a definite conclusion due to substantial statistical uncertainties. In fact, many neutrino DIS experiments were carried out with their own primary physical goals, for instance the structure of proton, the mixing angles of electro-weak interaction etc., but none of them can individually confirm the EMC effect.

Although there is no individual neutrino experiment on EMC effect, the differential cross sections and structure functions have been measured in neutrino-nucleus experiments in CCFR[66, 232] and NuTeV[68] at Fermilab, and in CDHSW[69] and CHORUS[70] at CERN. These experimental data would help us to understand the nuclear effects in the neutrino-nucleus interaction further.

Along with the experimental efforts, several groups have been performed theoretical as well as phenomenological analysis of the nuclear effects in neutrino-nucleus DIS. Among them most prominent are the Kulagin and Petti(KP)[223, 227], Qiu and Vitev(QV)[233] and Hirai, Komano and Nagai(HKN) groups, which have predicted the nuclear corrections in the low x region. Kulagin and Petti's approach is quite different from the above ones in the sense that they try to calculate the nuclear corrections in conventional nuclear models as far as they can, and then they try to attribute remaining factors to off-shell effects of bound nucleons for explaining the data.

8.3 Nuclear Shadowing Effect in the Non-singlet Structure Functions

In our previous chapters 4,5, and 6, we have calculated the non-singlet structure functions by means of solving DGLAP equations using two Regge ansatz as the initial input. Our calculations predicts the structure functions for a nucleon(single or free)

as

$$F_i(x,t) = F_i(x_0,t_0)\exp\left[\int_{t_0}^{t}\left(\frac{\alpha(t)}{2\pi}\right)_{NNLO} U(x_0,t)dt + \int_{t_0}^{t}\left(\frac{\alpha(t)}{2\pi}\right)^2_{NNLO} V(x_0,t)dt + \int_{t_0}^{t}\left(\frac{\alpha(t)}{2\pi}\right)^3_{NNLO} W(x_0,t)dt\right]\left(\frac{x}{x_0}\right)^{(1-bt)}. \tag{8.1}$$

However in predicting the free nucleon structure functions, we need to consider the input point $F_i(x_0,t_0)$, a free nucleon structure function at $x = x_0$ and $t = t_0$. In our previous analysis, the points were taken from the available experimental data. It is known that the experimental data for nucleon structure functions are extracted from nuclear targets and hence they are with several nuclear effects. Thus the experimental input points, we considered in our previous analysis are nothing but nuclear structure function $F_i^A(x_0,t_0)$, which in turn leads to inaccuracy in predicting free nucleon structure function. Therefore accurate prediction of free nucleon structure function requires a nuclear effect free input point.

The experimental results are the structure functions for bound nucleon F_i^A which is related to the free nucleon structure function as

$$R(x,t) = \frac{F^A(x,t)}{F^N(x,t)}. \tag{8.2}$$

Here $F^A(x,t)$ represents the nucleon structure function per nucleon and $F^N(x,t)$, the free nucleon structure function. At $x = x_0$ and $t = t_0$, if we consider the value of the nuclear correction factor to be $R(x,t) = R_0$, the input point in (8.1) can be replaced with $F_i^N(x_0,t_0) = \frac{F_i^A(x_0,t_0)}{R_0}$ and provides

$$F_i^N(x,t) = \frac{F_i^A(x_0,t_0)}{R_0}\exp\left[\int_{t_0}^{t}\left(\frac{\alpha(t)}{2\pi}\right)_{NNLO} U(x_0,t)dt + \int_{t_0}^{t}\left(\frac{\alpha(t)}{2\pi}\right)^2_{NNLO} V(x_0,t)dt + \int_{t_0}^{t}\left(\frac{\alpha(t)}{2\pi}\right)^3_{NNLO} W(x_0,t)dt\right]\left(\frac{x}{x_0}\right)^{(1-bt)}. \tag{8.3}$$

Structure functions/	Referred analysis	References
F_2^{NS}	S. A. Kulagin and R. Petti	[227]
xF_3	S. A Kulagin and R. Petti	[227]
xg_1^{NS}	V. Guzey and M. Strikman	[228]

Table 8.1: Summary of referred analysis in our study of nuclear effects in various structure functions and sum rules.

Above expression is capable of predicting the free nucleon structure function through the experimental data $F_i^A(x_0, t_0)$ along with the correction factor R_0.

Moreover, due to the unavailability of free nucleon structure function data, direct phenomenological analysis of (8.3) is not possible. In order to perform phenomenological analysis of our results with the experimental data either we need to remove nuclear effects from the data points or include the corresponding effects to our results of free nucleon. Here we have considered the later one, i.e., we have incorporated the nuclear correction factor $R(x)$ with our calculations as

$$F_i^A(x,t) = R(x)F_i^N(x,t) = R(x)\frac{F_i^A(x_0,t_0)}{R_0}\exp\left[\int_{t_0}^{t}\left(\frac{\alpha(t)}{2\pi}\right)_{NNLO} U(x_0,t)dt + \int_{t_0}^{t}\left(\frac{\alpha(t)}{2\pi}\right)^2_{NNLO} V(x_0,t)dt + \int_{t_0}^{t}\left(\frac{\alpha(t)}{2\pi}\right)^3_{NNLO} W(x_0,t)dt\right]\left(\frac{x}{x_0}\right)^{(1-bt)}, \quad (8.4)$$

in order to describe properly the experimental results.

The results for the nuclear correction factor $R(x)$ predicted in different analysis for different structure functions, which are utilized in our analysis are summarised in Table8.1. Incorporating these nuclear effects we have calculated the nuclear structure functions. Here we have also considered the fact that the nuclear effects in the non-singlet parts F_2^{NS} and g_1^{NS} are equivalent to the corresponding structure functions F_2 and g_1[55].

8.3.1 Shadowing Effect in $F_2^{NS}(x, Q^2)$

In accord with (8.4), our expressions obtained in chapter 4 for F_2^{NS} nucleon structure functions predicts the corresponding nuclear structure functions as

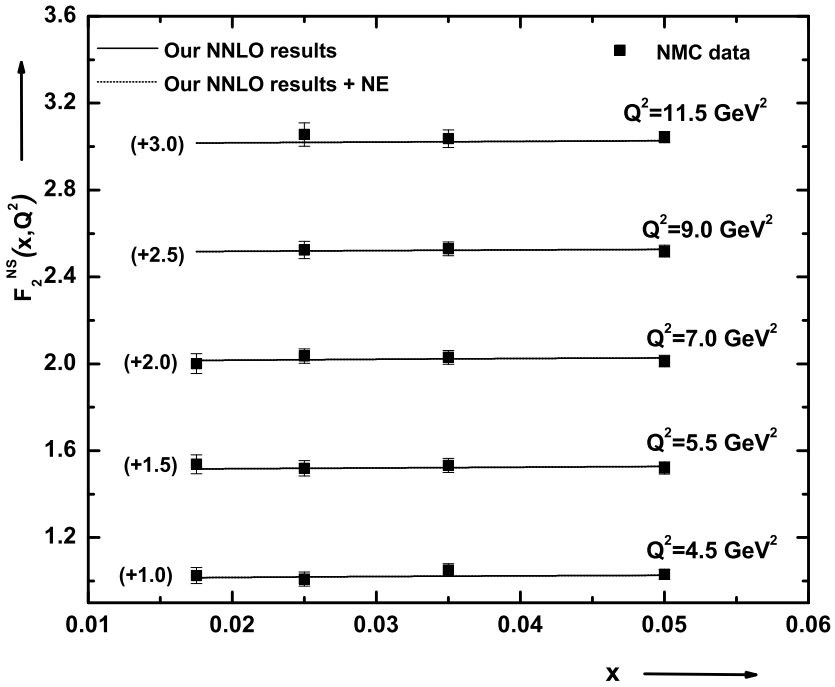

Figure 8.1: Our NNLO results for F_2^{NS} structure function with and without nuclear effect, in comparison with the NMC measurement.

$$F_2^{NS(A)}(x,t) = R_2(x)F_i^{NS(N)}(x,t) = R_2(x)\frac{F_2^{NS(A)}(x_0,t_0)}{R_0} \times \exp\left[\int_{t_0}^{t}\left(\frac{\alpha(t)}{2\pi}\right)_{NNLO} U(x_0,t)dt + \int_{t_0}^{t}\left(\frac{\alpha(t)}{2\pi}\right)^2_{NNLO} V(x_0,t)dt + \int_{t_0}^{t}\left(\frac{\alpha(t)}{2\pi}\right)^3_{NNLO} W(x_0,t)dt\right]\left(\frac{x}{x_0}\right)^{(1-bt)}. \quad (8.5)$$

In this regard we have used the results for nuclear correction factor, R_2 from Ref.[218, 227, 233]. Incorporating the corrections to our calculations of F_2^{NS} structure function, we have obtained the nuclear structure function $F_2^{NS(A)}$ and depicted it in Fig. 8.1. Here we have shown only the modification of our NNLO results in comparison with NMC experimental data. We observe that our results for free nucleon structure functions, along with nuclear effect predicted by KP provides a well description of available experimental data for nuclear structure functions.

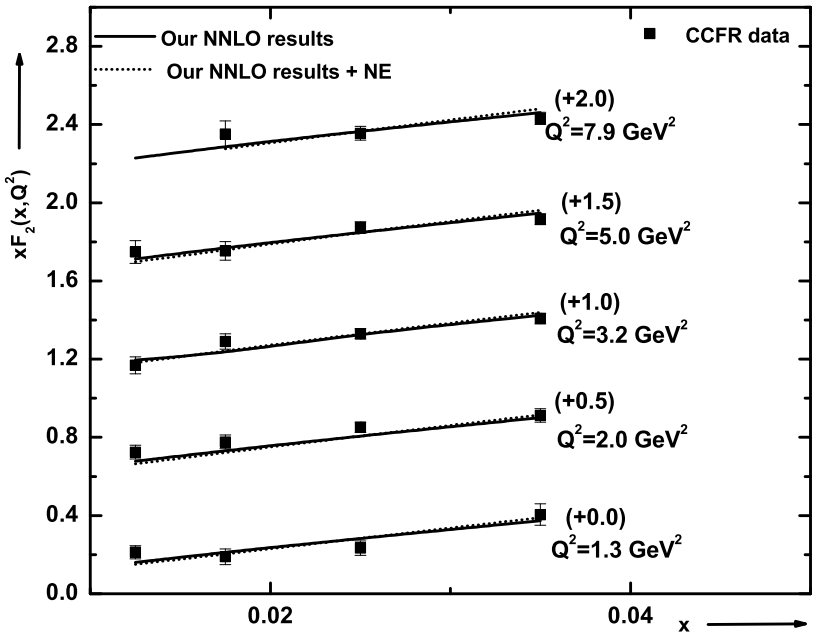

Figure 8.2: Our NNLO results for xF_3 structure function with and without nuclear effect, in comparison with the CCFR data.

8.3.2 Shadowing Effect in $xF_3^{NS}(x,Q^2)$

Our result (5.51) for xF_3 nucleon structure functions along with necessary corrections due to nuclear effect predicts the nuclear structure functions as

$$xF_3^{(A)}(x,t) = R_3(x)xF_3^{(N)}(x,t) = R_3(x)\frac{xF_3^{(A)}(x_0,t_0)}{R_0} \times \exp\left[\int_{t_0}^{t}\left(\frac{\alpha(t)}{2\pi}\right)_{NNLO} U(x_0,t)dt + \int_{t_0}^{t}\left(\frac{\alpha(t)}{2\pi}\right)^2_{NNLO} V(x_0,t)dt + \int_{t_0}^{t}\left(\frac{\alpha(t)}{2\pi}\right)^3_{NNLO} W(x_0,t)dt\right]\left(\frac{x}{x_0}\right)^{(1-bt)}. \quad (8.6)$$

In this case we have used the results for nuclear correction factor, R_3 from KP[227]. Incorporating the corresponding corrections to our calculations of xF_3 structure function, we have obtained the nuclear structure function $xF_3^{(A)}$ and depicted them in Fig. 8.2. Here we have shown only the modification of our NNLO results in comparison

--

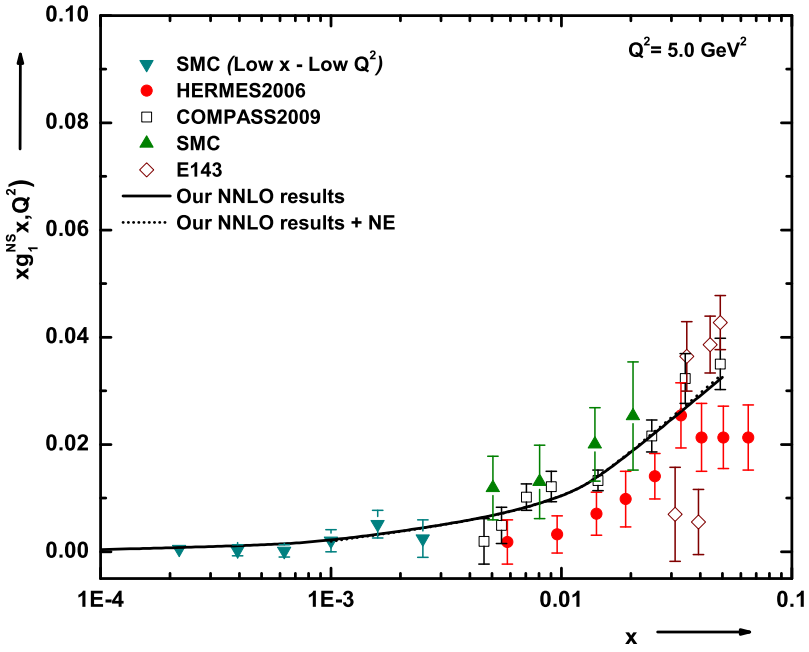

Figure 8.3: Our NNLO results for xg_1^{NS} structure function with and without nuclear effect, in comparison with SMC, HERMES, COMPASS and E143 data.

with CCFR, NuTeV, CHORUS and CDHSW experimental data. We observe that our results for free nucleon structure functions, along with nuclear effect predicted by KP provides a well description of available experimental data for nuclear structure functions.

8.3.3 Shadowing Effect in $xg_1^{NS}(x,Q^2)$

Similarly using the results for R_g obtained in [228] we can obtain the spin dependent nonsinglet nuclear structure functions as

$$xg_1^{NS(A)}(x,t) = R_g(x) xg_1^{NS(N)}(x,t) = R_g(x)\frac{xg_1^{NS(A)}(x_0,t_0)}{R_g} \times \exp\left[\int_{t_0}^{t}\left(\frac{\alpha(t)}{2\pi}\right)_{NNLO} U(x_0,t)dt + \int_{t_0}^{t}\left(\frac{\alpha(t)}{2\pi}\right)^2_{NNLO} V(x_0,t)dt + \int_{t_0}^{t}\left(\frac{\alpha(t)}{2\pi}\right)^3_{NNLO} W(x_0,t)dt\right]\left(\frac{x}{x_0}\right)^{(1-bt)}. \quad (8.7)$$

The results for (8.7) are depicted in Fig. 8.3. In this regard our results including nuclear effects are observed to be compatible with the experimetal data.

8.4 Shadowing Effect in the Sum Rules

Analogous to the structure functions, experimental determination of the DIS sum rules consists of considerable nuclear effects. As DIS sum rules are associated with the underlying symmetry as well as conservation laws of interactions, they provide strong normalization constraints on the structure functions. Therefore the sum rules are expected to provide an important bridge between different nuclear effects.

In this section we briefly discuss the nuclear effects in DIS sum rules, specifically in the GSR, GLSSR and BSR based on several earlier analysis. We then incorporate possible nuclear corrections to our results of sum rules, obtained in the previous chapter and perform phenomenological analysis in comparison with the experimental measurements.

8.4.1 Shadowing Correction to Gottfried Sum Rule

In the NMC experiment, due to the unavailability of fixed target for neutron, deuteron is usually used for measuring neutron structure function and combining the relations

$$F_2^p - F_2^n = 2F_2^d \frac{1 - F_2^n/F_2^p}{1 + F_2^n/F_2^p}, \tag{8.8}$$

$$\frac{F_2^n}{F_2^p} = 2\frac{F_2^d}{F_2^p} - 1 \tag{8.9}$$

and

$$F_2^d = F_2^p + F_2^n \tag{8.10}$$

together with world averaged deuteron structure functions, the difference $F_2^p - F_2^n$ is calculated and these calculations are used in determining the GSR. The results can be compared with the GSR only if there is no nuclear modification in the deuteron. However it is well known that nuclear structure functions are modified and the major contribution to the modification comes from the small-x region i.e., shadowing region. Nuclear corrections in the deuteron to the GSR, in particular the shadowing effect, were

calculated in various models[234–240]. So far, VMD, Pomeron and meson-exchange mechanisms have been studied. In Ref. [240], using VMD model, including ρ, ω and ϕ as the vector mesons, estimated the shadowing correction $\delta S_{GSR} = -0.039 to -0.017$ to the GSR $S_{GSR} = S_{GSR}^{NMC} + \delta S_{GSR}$. There are other studies in the Pomeron and meson exchange models. Historically, the first estimate of shadowing contribution to S_{GSR} is discussed by the Pomeron exchange model[234, 235]. A possible way of describing the high-energy scattering in the diffractive region is in terms of Pomeron exchange. The virtual photon transforms into a $q\bar{q}$ pair which then interacts with the deuteron. In the diffractive case, the target is remain intact and only vacuum quantum number, namely the Pomeron, could be exchanged between the $q\bar{q}$ pair and the nucleons. In the earlier works, the shadowing correction in this model was rather large $\delta S_{GSR} \approx -0.08$ [235, 238]. However, the Pomeron contribution is reduced if more realistic deuteron wave functions are used according to Ref. [239]. Next, meson-exchange corrections were investigated in Refs. [236,239]. The studied mesons are π, ω and σ in Ref. [236], and ρ is also included in Ref.[239]. If the corrections due to the π, ω and σ mesons were taken into account, the NMC result became $S_{GSR} = 0.29 \pm 0.03$ [236]. Therefore, meson-exchange contributions reduce the discrepancy between the NMC data and the Gottfried sum rule.

As far Figs.7.2, 7.3 and 7.4 are concerned, it is observed that our results do not agree well with the available experimental data of NMC. Again as the nuclear effects predicted by the available analysis(discussed above), are observed to be large and inclusion of these effects to our results will deviate from the experimental data farther, hence we have not included the nuclear corrections to our results of GSR.

8.4.2 Shadowing Correction to GLS Sum Rule

Experimental measurements of GLS sum rule was performed by CCFR and the results were extracted from Fe target. In order to compare our results for GLS sum rule obtained in chapter7, we refer the nuclear corrections estimated in [223, 241]. The detailed investigation on the nuclear corrections to GLS sum rule was performed in Ref. [223]. They explicitly separated the nuclear corrections to the GLS integral as $S_{GLS}^{A} = S_{GLS}^{N} + \delta S_{GLS}$, where S_{GLS}^{N} refers to the GLS integral for nucleon. In accord with their predictions, the nuclear corrections to the GLS sum rule cancel out as $x \to 0$ in the leading order, which is due to the baryon charge conservation. They have also calculated the GLS integral S_{GLS} for different nuclear targets. In Ref. [223, 241],

they obtained the corrections for iron and deuteron nuclei as $\frac{\delta S^{Fe}_{GLS}}{3} = -\frac{4.0\times10^{-3}}{Q^2}$ and $\frac{\delta S^{D}_{GLS}}{3} = -\frac{6.3\times10^{-4}}{Q^2}$ respectively. In Ref. [223] they have nicely presented their result in Fig. 10. From Fig. 10 we observe that the nuclear correction δ_{GLS} decreases progressively by increasing Q^2.

The GLS sum rule for nuclei can be expressed as

$$S^{A}_{GLS}(x_{min}, Q^2)\Big|_{NNLO} = S^{N}_{GLS}(Q^2) + \delta S_{GLS}, \tag{8.11}$$

where the first term on the right hand side of above equation represents the GLS sum rule for free nucleon and the second term for the nuclear correction. Using the NNLO pQCD corrected expression 7.17, obtained in chapter 7 as $S^{N}_{GLS}(Q^2)$ we get

$$\begin{aligned} S^{A}_{GLS}(x_{min}, Q^2)\Big|_{NNLO} = S_{GLS}(Q^2)\Big|_{NNLO} - \int_0^{x_{min}} \frac{dx}{x}\Bigg[F_3^{NS}(x_0,t_0)\left(\frac{x}{x_0}\right)^{(1-bt)} \\ \exp\Bigg\{\int_{t_0}^{t}\left(\frac{\alpha(t)}{2\pi}\right)_{NNLO} \\ P(x_0,t)dt + \int_{t_0}^{t}\left(\frac{\alpha(t)}{2\pi}\right)^2_{NNLO} Q(x_0,t)dt \\ + \int_{t_0}^{t}\left(\frac{\alpha(t)}{2\pi}\right)^3_{NNLO} R(x_0,t)dt\Bigg\}\Bigg] + \delta S_{GLS}. \end{aligned} \tag{8.12}$$

Now incorporating the KP[223, 241] prediction $\frac{\delta S^{Fe}_{GLS}}{3} = -\frac{4.0\times10^{-3}}{Q^2}$, for the nuclear correction term, we have calculated S^{A}_{GLS} and depicted the results in Fig. 8.4, in comparison with CCFR measurements of xF_3 structure function with Fe as the target. In addition, we have plotted our NNLO results and the results of KS[179] prediction. From the figure we see that the our NNLO expression for GLSSR along with necessary nuclear correction has the capability of describing the experimental data of GLSSR for nuclei.

8.4.3 Shadowing Correction to Bjorken Sum Rule

Aiming at measuring the polarized structure functions of protons and neutrons and in order to test the Bjorken sum rule several experiment have been performed. The measurement of $g_1^n(x)$ involves necessarily nuclear targets and several experiments have been performed using ^2H and ^3He targets. However ^3He target has advantage

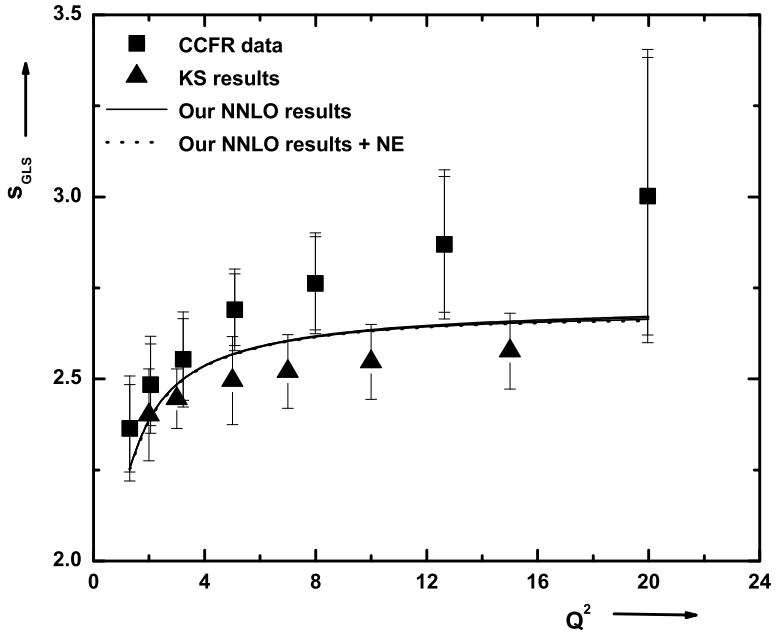

Figure 8.4: Our NNLO results for Gross-Llewelln Smith sum rule with and without nuclear effect, in comparison with those of CCFR measurements. (Q^2's are taken in the unit of GeV^2).

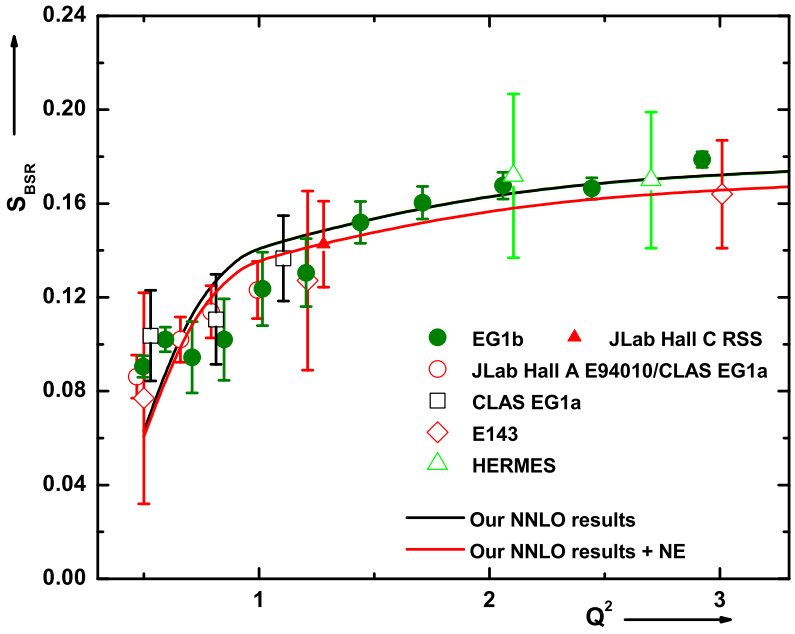

Figure 8.5: Our NNLO results for Bjorken sum rule with and without nuclear effect, in comparison with several experimental data as indicated in the figure. (Q^2's are taken in the unit of GeV^2).

over ^2H target. On the other hand the use of heavy nucleus as target yields nuclear effects. Nuclear effects for the Bjorken sum rule were first discussed in Ref. [242] and Ref. [243]. In particular it was pointed out in Ref. [243] that convolution models and three nucleon description of $A = 3$ system lead to results for $g_{1A=3}$ inconsistent with the Bjorken sum rule. This observation was left unnoticed in Ref. [244, 245] and in all analyses of the experimental data. In Ref.[55], the ratio of the Bjorken sum rule for $A = 3$ to $A = 1$ within impulse approximation was found to be

$$R = \frac{\int_0^1 dx \Big[g_1^{He}(x,Q^2) - g_1^H(x,Q^2) \Big]}{\int_0^1 dx \Big[g_1^n(x,Q^2) - g_1^p(x,Q^2) \Big]} = \frac{G_A^{^3H}}{G_A(n)}, \tag{8.13}$$

where G_A is the axial coupling constant for β decay of the nucleus A. Combining the most recent experimental data on $\frac{G_A^{^3H}}{G_A(n)}$ for tritium β-decay [246] it was found to be $\frac{G_A^{^3H}}{G_A(n)} = 0.9634 \pm 0.003$. However, for the case of ^7Li the ratio was obtained to be 0.73. Further in Ref. [55], this value was estimated to be $\frac{G_A^{^3H}}{G_A(n)} = 0.922 \pm 0.006$.

Using the values of $\frac{G_A^{^3H}}{G_A(n)}$ obtained in Ref. [55, 246], we can calculate the BSR integral $S_{BSR}^A = \int_0^1 dx \Big[g_1^{He}(x,Q^2) - g_1^H(x,Q^2) \Big]$ using our NNLO results for $S_{BSR} = \int_0^1 dx \Big[g_1^n(x,Q^2) - g_1^p(x,Q^2) \Big]$, obtained in chapter 7 as

$$\begin{aligned} S_{BSR}^A = \frac{G_A^{^3H}}{G_A(n)} \Bigg[S_{BSR}(Q^2)\Big|_{NNLO} - \int_0^{x_{min}} \frac{dx}{x} \Bigg[g^{NS}(x_0,t_0) \left(\frac{x}{x_0}\right)^{(1-bt)} \times \\ \exp\Bigg\{ \int_{t_0}^t \left(\frac{\alpha(t)}{2\pi}\right)_{NLO} P(x_0,t)dt + \int_{t_0}^t \left(\frac{\alpha(t)}{2\pi}\right)_{NLO}^2 Q(x_0,t)dt \Bigg\} \\ + \int_{t_0}^t \left(\frac{\alpha(t)}{2\pi}\right)_{NNLO}^3 R(x_0,t)dt \Bigg\} \Bigg] \Bigg]. \end{aligned} \tag{8.14}$$

In Fig. 8.5, we have shown the results for BSR in accord with Eq.(8.14) along with other experimental. Nuclear correction incorporated results are observed to be consistent with other measurements.

8.5 Summary

In this chapter we present an analysis of the non-singlet structure functions and related sum rules taking into account the nuclear effects. In this regard, special

attention is given to the nuclear shadowing effect as we are mostly concerning with the small-x region. Incorporating the results of corrections due to shadowing nuclear effect obtained in several earlier analysis for different structure functions as well as sum rules to our results of the structure functions and sum rules for free nucleon, we obtain structure functions and sum rules for nuclei. Nuclear correction incorporated results are studied phenomenologically and it is observed that along with the nuclear correction, our NNLO results of the non-singlet structure functions and sum rules have the capability of providing well description of their respective experimental data collected using nuclear target. capable of describing well the obtained in previous chapters analysis in comparison with the available data and parametrization. □□